Journal Pre-proofs

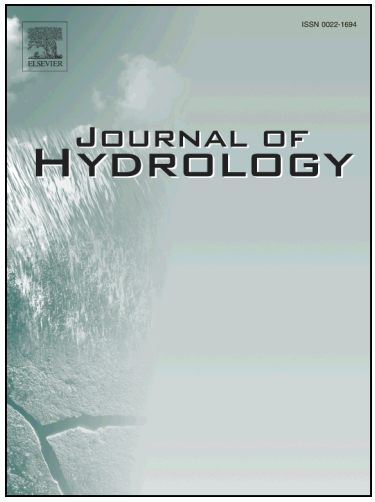

Research papers

Temporal variations in porewater fluxes to a coastal lagoon driven by wind waves and changes in lagoon water depths

Valentí Rodellas, Peter G. Cook, James McCallum, Aladin Andrisoa, Samuel Meulé, Thomas C. Stieglitz

PII: S0022-1694(19)31098-4
DOI: https://doi.org/10.1016/j.jhydrol.2019.124363
Reference: HYDROL 124363

To appear in: *Journal of Hydrology*

Received Date: 3 October 2019
Revised Date: 4 November 2019
Accepted Date: 13 November 2019

Please cite this article as: Rodellas, V., Cook, P.G., McCallum, J., Andrisoa, A., Meulé, S., Stieglitz, T.C., Temporal variations in porewater fluxes to a coastal lagoon driven by wind waves and changes in lagoon water depths, *Journal of Hydrology* (2019), doi: https://doi.org/10.1016/j.jhydrol.2019.124363

Temporal variations in porewater fluxes to a coastal lagoon driven by wind waves and changes in lagoon water depths

Valentí Rodellas[1,2*], Peter G. Cook[3,4], James McCallum[5], Aladin Andrisoa[1], Samuel Meulé[1], Thomas C. Stieglitz[1,6]

[1]Aix-Marseille Univ, CNRS, IRD, INRA, Coll France, CEREGE, 13545 Aix-en-Provence, France

[2]Institut de Ciència i Tecnologia Ambientals (ICTA), Universitat Autònoma de Barcelona, E-08193 Bellaterra, Catalonia, Spain

[3]National Centre for Groundwater Research and Training (NCGRT), School of the Environment, Flinders University, Adelaide SA 5001, Australia

[4]Aix-Marseille Université, IMéRA, 13000 Marseille, France

[5]School of Earth Sciences, The University of Western Australia, Perth WA 6009, Australia

[6]Centre for Tropical Water and Aquatic Ecosystem Research, James Cook University, Townsville, Queensland 4811, Australia

*Corresponding Author: Valentí Rodellas (valenti.rodellas@uab.cat)

ABSTRACT

Porewater fluxes, including fresh groundwater discharge and circulation of surface waters through sediments, are increasingly documented to play an important role in hydrological and biogeochemical cycles of coastal water bodies. In most studies, the magnitude of porewater fluxes is inferred from geochemical tracers, but a detailed understanding of the underlying physical forces driving these fluxes remains limited. In this study, we evaluate the mechanisms driving porewater fluxes in the shallow coastal La Palme lagoon (France). We combined measurements of variations of salinity and temperature in the subsurface with 1-dimensional fluid, salt and heat transport models to evaluate the dynamics of porewater fluxes across the sediment-water interface in response to temporally variable forcings. Two main processes were identified as major drivers of porewater fluxes: i) temporal variations of lagoon water depths (forcing porewater fluxes up to 25 cm d^{-1}) and ii) locally-generated wind waves (porewater fluxes of ~50 cm d^{-1}). These processes operate over different spatial and temporal scales; Wind-driven waves force the shallow circulation of surface lagoon waters through sediments (mostly < 0.2 m), but are restricted to strong wind events (typically lasting for 1-3 days). In contrast, porewater fluxes driven by variations of lagoon water depths flush a much greater depth of sediment (>1 m). The spatial and temporal scales of driving forces will largely determine the significance of porewater fluxes, as well as their chemical composition. Thus, an appropriate evaluation of the magnitude of porewater-driven solute fluxes and their consequences for coastal ecosystems requires a solid and site-specific understanding of the underlying physical forces.

Keywords: porewater exchange, submarine groundwater discharge, coastal lagoon, driving forces, waves, salinity, temperature

1. INTRODUCTION

Water fluxes circulating through permeable sediments are increasingly being recognized as an important source of dissolved solutes (e.g. nutrients, metals, pollutants) to surface water bodies (Anschutz et al., 2009; Liefer et al., 2013; Rodellas et al., 2015). In coastal settings, these fluxes across the sediment-water interface are commonly referred to as Submarine Groundwater Discharge (SGD) or porewater exchange (PEX), depending on the scale of the circulation process (Moore, 2010; Santos et al., 2012). In this study, we use the term porewater fluxes to refer to the total efflux of water and solutes across the permeable sediments to surface waters, thus including both SGD and PEX. Porewater-driven fluxes of solutes may exert a major control on the biogeochemistry, water quality and ecological functioning of receiving water bodies, e.g. contributing to sustaining the primary production and community composition of phytoplankton in coastal areas (Andrisoa et al., 2019; Garcés et al., 2011; Valiela et al., 1990), promoting eutrophication of surface waters (Hwang et al., 2005; Paerl, 1997), and leading to recurrent harmful algal blooms (Gobler and Sañudo-Wilhelmy, 2001; Lee et al., 2010).

The physical mechanisms driving porewater fluxes strongly affect the residence time of waters within sediments or the coastal aquifer, determining the extent and rates of biogeochemical reactions and therefore the composition of discharging fluids (Santos et al., 2012; Weinstein et al., 2011). An appropriate understanding of the magnitude of solute fluxes driven by groundwater and porewater discharge requires thus identifying the mechanism forcing these inputs. Many physical processes produce pressure gradients at the sediment-water interface that can force advective porewater fluxes. The main driving forces include the terrestrial hydraulic gradient and its seasonal oscillations, wave and tidal pumping, the interaction of currents and seafloor topography, convection

driven by density inversions or pumping activities of benthic fauna (Huettel et al., 2014; Santos et al., 2012). These different forcing mechanisms, which are of both marine (e.g. wave and tidal setup) and terrestrial (e.g. hydraulic gradient) origin, are highly dynamic and irregular, span a wide range of exchange lengths and timescales and are frequently superimposed (Robinson et al., 2017; Santos et al., 2012, 2009).

A large number of studies highlight the overall magnitude and the significance of porewater fluxes (e.g. (Cho et al., 2018; Kwon et al., 2014; Moore et al., 2008; Rodellas et al., 2015)), but there is still little information about their driving forces (Robinson et al., 2017). Studies conducted to date have evaluated the effect of individual driving forces in isolation and have been mainly focused on regular and short-term forces (e.g. semi-diurnal/diurnal tides, density-driven flows), mainly as a consequence of the difficulties inherent in investigating irregular and longer period forcing via field experiments and in unraveling the various forcing effects (Robinson et al., 2017). Irregular forcings, such as episodic, high intensity events, may have a great impact on fluxes of water and solutes driven by porewater fluxes (Sawyer et al., 2013; Smith et al., 2008). The understanding of these forcing is thus required to better predict the effects of increasing stressors in the system (e.g. climate change, anthropogenic pressure) and to better identify settings where specific forcings may dominate over the others.

This study is aimed at characterizing porewater fluxes in a shallow coastal lagoon (La Palme Lagoon, France), where the circulation of significant volumes of surface water through sediments have been previously documented (Cook et al., 2018a; Rodellas et al., 2018; Stieglitz et al., 2013; Tamborski et al., 2018). These previous studies have estimated the average magnitude of porewater fluxes to the lagoon, but they provided

little insight into their temporal variations and the mechanisms driving these fluxes. The current paper examines variations of subsurface temperature and porewater salinity in La Palme lagoon to evaluate the dynamics of porewater fluxes and to provide some insight into controlling forcings. In this study, we focus on two mechanisms that can control porewater fluxes in the lagoon and that operate over different temporal and spatial scales: i) the variations of lagoon water depths, which can influence the terrestrial hydraulic gradient and drive long-scale (>1 m) porewater fluxes, and ii) wave pumping produced by the strong winds of the region, which forces the flushing of shallow sediments (short-scale porewater fluxes). Other active mechanisms are likely significantly contributing to total porewater fluxes (e.g. bioirrigation or current-topography interactions), but they are not specifically evaluated in this study.

2. METHODS

2.1. Study site: La Palme lagoon, France

La Palme is a small (500 ha surface area), shallow coastal lagoon, with mean and maximum water depths of ~0.7 and ~2 m, respectively (Fig. 1). It is connected with the Mediterranean Sea through a small opening in the coastal sand spit, which may be seasonally closed, and it receives continuous fresh groundwater inputs (0.01 – 0.04 $m^3 s^{-1}$) mainly from a regional karst aquifer, constituted by karstified Jurassic and Lower Cretaceous limestones (Stieglitz et al., 2013; Wilke and Boutière, 2000). The lagoon is also connected with a shallow alluvial aquifer (Alluvial aquifer of Aude and Berre rivers), but little information is available on the aquifer-lagoon interaction. The internal mixing of the lagoon and its exchange with coastal waters is driven primarily by the strong north-westerly winds characteristic of the region (regularly exceeding 10 m s^{-1}). Given that tidal variations in the Mediterranean Sea are usually small and the exchange between La Palme lagoon and the sea is highly restricted by three physical barriers (railway dike, road dike and sandy barrier; Fig. 1), tidal forcing plays a minor role on the hydrodynamic functioning of this lagoon (tidal range in the lagoon <1cm; (Fiandrino et al., 2012)). Most of the lagoon is covered by fine-to-coarse grained sands (100-500 μm) and only the northern part of the lagoon is dominated by fine-grained sediments (~50 μm). The eastern part of the lagoon is surrounded by evaporation ponds, but there is no visual or chemical evidence of a connection between the lagoon and the salt pond (Rodellas et al., 2018; Tamborski et al., 2018).

A study conducted by Stieglitz et al. (2013) hypothesized that strong winds produced circulation of large amounts of lagoon water through surface sediments. Different studies have estimated porewater inputs to the entire lagoon at 0.4 – 2.1 $m^3 s^{-1}$ (0.8 – 4.1 cm d^{-1}),

which is the equivalent of the volume of the entire lagoon circulating through the sediments every 20 - 90 days (Rodellas et al., 2018; Stieglitz et al., 2013; Tamborski et al., 2018). However, to date, the forces driving these fluxes have not been evaluated in detail.

2.2. Sampling and analysis

Four different stations (Pz1, Pz2, Pz3, Pz4) were established in areas considered representative of the different sediment types of the lagoon (Fig 1). In May 2017, a sediment core (up to 50 cm depth) was collected at each one of these locations and sliced every 5 cm. The grain size distribution of each sediment sample was determined through a Coulter LS230 laser diffraction particle size analyzer. Average sediment porosities for each location were obtained from Tamborski et al. (2018), who collected sediment cores at the same locations. Sensors for measuring temperature, salinity, lagoon water depths and wave parameters were also installed at these sites and porewater samples were collected, as discussed in the following sections.

Hourly rainfall, temperature, wind (speed and direction) and atmospheric pressure data at the nearby meteorological station “Leucate” was extracted from the database of the French meteorological service (Météo France). Additional monthly data on lagoon water depths and salinity at three sites in the northern lagoon (PN stations in Fig. 1) was obtained from the database of “Parc Naturel Régional de la Narbonnaise en Méditerranée” (PNRNM). Data on daily piezometric levels of the alluvial aquifer connected to the lagoon (Alluvial aquifer of Aude and Berre rivers) was obtained from the French Groundwater National Portal (piezometer code BSS002LRH; ades.eaufrance.fr).

2.2.1. Subsurface salinity time series

Porewater samples for salinity analysis were collected during 7 different sampling campaigns between March 2016 and June 2017 (March, April, June, October and November 2016; April and June 2017). During each campaign, porewater samples were collected from 3 different locations (Pz1, Pz2 and Pz3) using a direct-push, shielded-screen well-point piezometer (Charette and Allen, 2006). Porewater samples for salinity analysis (10 mL) were collected at depths ranging from 5 to 140 cm below the sediment-water interface (including surface water) and measured using a pre-calibrated WTW multiparameter sonde (WTW Multi 3430 meter with TetraCon® 925 probe).

A CTD logger (LTC Levelogger® from Solinst®) was installed at Pz1 from 1st April 2017 to 31st December 2017 at 10 cm above the sediment-water interface to monitor water level (measurements were corrected for atmospheric pressure) and salinity variations in surface waters. Additionally, a CTD logger (LTC Levelogger® from Solinst®) was placed at 30 cm below the sediment-water interface to record changes in porewater salinities at this depth for the same period. This logger was driven into sediments by using a plastic rod with a shielded protection to avoid clogging of the conductivity cell (which was also protected with a membrane) during installation and to minimize the disturbance of sediments. Changes in pressure were also recorded at 30 cm below the sediment-water interface, but water level gradients between this depth and surface water were too small to be measured.

2.2.2. Subsurface temperature time series

In situ temperature data was acquired by a string of Thermochron iButton© thermistors (Measuring Systems Ltd), which are small-size, stand-alone and inexpensive temperature loggers with a reported accuracy of ±0.2ºC and a resolution of 0.06 ºC (Johnson et al.,

2005). The sensors were placed at depths of 5, 10, 15, 25 and 40 cm below the sediment-water interface and at 10 cm above the seafloor by vertically driving a 2 cm diameter wooden rod (with the thermistors inserted) into the sediments. These strings of thermistors were installed simultaneously at each of the above 4 locations in La Palme lagoon (Pz1, Pz2, Pz3, Pz4) during 2 periods of ~1 month (between May 9 and May 30, and between June 9 and July 5). The strings of thermistors were also installed between November and December 2017, but the data obtained from this deployment is not included in this manuscript because it was a period of abrupt changes in lagoon water depths which makes interpretation of the data difficult. Once recovered, the thermistors were intercalibrated in a calibration bath. During the deployment periods, pressure sensors (NKE, SP2T10) were installed at stations Pz1, Pz2 and Pz3 measuring water depths for 5 minutes per hour at a frequency of 4Hz to monitor the variability of wave parameters (significant wave height and period) and water depths. A barometer (Barologger Edge from Solinst®) was also installed in La Palme lagoon to correct water pressures for changes in atmospheric pressure.

2.3. Numerical modeling

2.3.1. Numerical modeling of subsurface salinities to estimate deep porewater fluxes

Models of salt transport have been used to estimate the exchange of water and solutes across the sediment-water interface, where surface and porewaters have distinctive salt concentrations (Martin et al., 2007, 2004; Morris, 1995; Rapaglia and Bokuniewicz, 2009). A vertical one-dimensional finite element model was developed to investigate porewater fluxes from the subsurface to the lagoon, based on the equations of (Simmons et al., 2001; Voss and Souza, 1987). The fluid mass balance equation is:

$$\rho S_{op}\frac{\partial p}{\partial t} + \theta\frac{\partial \rho \partial C}{\partial C \partial t} + \frac{\partial}{\partial z}(\theta \rho v) = Q_p \qquad (1)$$

where ρ is the fluid density [kg m^3], S_{op} is the compressibility of the saturated sediment [Pa^{-1}], p is pressure [Pa], θ is the porosity [dimensionless], C is the concentration of the chemical species (salt) [kg m^{-3}], Q_p is the water source or sink [kg m^{-3} s^{-1}] and v is the fluid velocity [m s^{-1}] defined as:

$$v = -\left(\frac{k}{\mu\theta}\left[\frac{\partial p}{\partial z} - \rho g\right]\right) \qquad (2)$$

where k is the permeability of the sediment [m^2], μ is the viscosity of the fluid [Pa s] and g is the gravitational constant [9.8 m s^{-2}],

To simulate the movement of the solute species (salt, in this case), Equation 1 is coupled to the transport equation (Simmons et al., 2001; Voss and Souza, 1987):

$$\theta\rho\frac{\partial C}{\partial t} + \frac{\partial}{\partial z}\theta\rho v C - \frac{\partial}{\partial z}\left(\theta\rho D\frac{\partial C}{\partial z}\right) = Q_p(C_p - C) \qquad (3)$$

where D is the dispersion coefficient [m^2 s^{-1}] and C_p is the concentration of solute species (salt) in the fluid source [kg m^{-3}].

The equations were solved with a Galerkin finite element numerical technique using one-dimensional linear element, which was implemented in Python using the NumPy and SciPy libraries (Oliphant, 2007; van der Walt et al., 2011). The fluid (Eq. 1) and solute (Eq. 3) transport equations were solved iteratively until the residuals for both pressure and concentration were <10^{-9}. The term $\partial\rho/\partial C$ was assumed to be a constant value.

Parameter values used in the one-dimensional model are shown in Table 1. The model was assumed to be homogeneous, with uniform properties for permeability, viscosity, porosity and dispersity. The model implemented boundary conditions of pressure and

concentration at both the top and bottom node of the model, with pressure approximated as $p \approx \rho g h$. The water flux exchanged across the sediment-water interface (cm d^{-1} or cm^3 cm^{-2} d^{-1}) was assessed by determining the Darcy flux ($v\,\theta$) in the uppermost element. The model was set with element length of 0.05 m between the lagoon bed and 1 m depth, 0.1 m between 1 and 2 m, and 0.2 m between 2 and 4 m depth. These depths were chosen so that nodes were coincident with the location of porewater observations. The upper pressure and salinity boundary conditions were taken from measured values in the lagoon (see 2.2.1); Between 21st January 2016 and 29th June 2017, boundary conditions were obtained by linearly interpolating between monthly measurements in station PN1. Between 29th June 2017 and 31st December 2017, the salinity and pressure values were obtained from the CTD logger installed in the surface water at station Pz1 (see 2.2.1). The lower boundary condition was fixed at a constant salinity for the duration of the simulation; however, the lower pressure boundary was linearly varied over 6-month periods as part of model calibration. Notice that the variations in lower pressure boundary essentially represent variations in the inland groundwater head that are transmitted to lagoon sediments. The model was implemented with a 4-hours time step with a total simulation period of two years.

Calibration was undertaken by fitting the model results to the porewater depth profiles and the CTD logger data at 0.3 m depth. All of the parameters were fixed for the calibration, with the exception of h_{bot}, C_{bot}, k, θ and α. Calibration was undertaken using the truncated Newton method (Nash, 1984), implemented in SciPy (Oliphant, 2007). The adjustable parameters (h_{bot}, C_{bot}, k, θ and α) were modified to reduce the misfit between the modeled and observed values of salinity at depth. This model was only implemented at station Pz1 because it was the only station where all the input data needed for the

model was collected (e.g. porewater depth profiles, surface salinities and water depths, continuous data at 0.3 m). The initial concentration profile was determined by linearly interpolating between the measured concentrations and the lower boundary conditions to produce a continuous concentration profile. This initial concentration profile was used to generate a steady state pressure distribution in the profile to use as the starting conditions for the transient model simulation. This was achieved by solving Eq. 1 where the variation of concentration and pressure with time were set to zero.

2.3.2. Numerical modeling of subsurface temperatures to estimate shallow porewater fluxes

Heat has been used as an environmental tracer for investigating groundwater, porewater and surface water interactions in a range of hydrogeologic settings (Boano et al., 2014; Cranswick et al., 2014; Martin et al., 2006; Savidge et al., 2016). Its application is based on temperature differences between surface water bodies, which are subject to diel or seasonal temperature variations, and porewater or groundwaters, which typically display reduced temperature variation (Cranswick et al., 2014). Most of the studies have applied the heat transport equation in thermal porewater records to estimate groundwater advection. However, it can also be applied to estimate shallow rapid porewater exchange by using a 1-D enhanced dispersion term that includes (aside from thermal conductivity) an effective dispersion term accounting for the increase of heat transport driven by porewater exchange (Bhaskar et al., 2012; Wilson et al., 2016). In a system without net groundwater advection, the enhanced dispersion coefficient can be obtained using:

$$\frac{\partial \mathrm{T}}{\partial \mathrm{t}} = \mathrm{D_e}\frac{\partial^2 \mathrm{T}}{\partial \mathrm{z}^2} \qquad (4)$$

where T is temperature, t is time, z is depth and D_e is the enhanced dispersion coefficient.

A finite difference model was written in Fortran 95 to solve Eq. 4. Rather than calibrating the model to observed temperatures at all depths simultaneously, we chose to calibrate temperature at each depth separately for discrete 48-hour periods with relatively constant wave conditions. A period of 48 hours was chosen because periods of high wind of much longer duration did not occur during our periods of measurement and shorter periods are less likely to induce significant temperature changes in the subsurface. To evaluate the relevance of wave pumping as a driver of porewater fluxes, several 48-hour periods during the different monitoring periods were selected to represent both high and low wind (wave) conditions.

Although shallow porewater fluxes are likely to produce an effective dispersion coefficient that decreases with depth (Qian et al., 2009; Wilson et al., 2016), we model the data using a constant dispersion coefficient, but model the temperature at each depth separately. The best-fit dispersion coefficient (D_e) therefore represents a combination of conduction and the apparent dispersion coefficient due to porewater exchange fluxes, to the relevant depth. The model was run for each of the selected 48-hour periods, and each piezometer and depth using different values of D_e (in increments of $3.5 \cdot 10^{-4}$ m^2 d^{-1}). The lowest RMSE (Root Mean Square Error) value in each case identified the best-fit value of D_e. Uncertainties associated with dispersion coefficients were estimated based on the shape of the RMSE versus D_e plot for each piezometer and each 48-hour period. Considering the accuracy of the temperature sensors (0.2 ºC), upper and lower bounds were defined by RMSE values 0.1 ºC greater than the minimum RMSE in each case. Considering the little dependence of thermal conductivity on salinity (Caldwell, 1974), we assume that variations of porewater salinities have a negligible influence on the computations.

The time for temperature changes in surface water to propagate into the subsurface can be expressed as:

$$t = \frac{z^2}{4D_e} \qquad (5)$$

Thus, for $D_e = 4 \cdot 10^{-2}$ m^2 d^{-1} (a typical value for enhanced dispersion coefficient due to wind and wave action; see below), the time for surface water temperature changes to propagate to depths (z) of 5, 10, 15, 25 and 40 cm (depths at which sensors were installed) is 0.4, 1.5, 3.3, 9.3 and 24 hours, respectively. We thus chose to focus on depths of 10 and 15 cm, as temperatures at greater depths do not respond sufficiently to wave conditions within the 48-hour period. We also discarded the sensors at 5 cm because of uncertainties in the depth of installation and the potential effects of artifacts associated with the installation of the wooden rod (e.g. alteration of sediment-water interface).

To calibrate the model, the upper boundary condition was specified as the measured surface water temperature (sensor at 10 cm above the sediment-water interface), and a constant temperature (20 ºC) was specified at a depth of 20 m. By using temperature in surface water as upper boundary condition, we are assuming that potential solar heating of sediments has a minor influence on the heat balance. The initial condition was specified to be the measured temperatures at the start of each period, with linear interpolation between observation depths. Initial temperatures between the deepest sensor and the model lower boundary at 20 m were also determined by linear interpolation between the deepest measurement and the specified lower boundary temperature. Varying the temperature value of the lower boundary confirmed that this did not affect simulated temperatures at the observation depths. Depth discretisation was 0.005 m, and temporal discretisation was $3.5 \cdot 10^{-5}$ d (0.05 min).

Fig. 2 shows how different values of D_e affect time series of temperature at 15 cm depth. Lower D_e values result in reduced diurnal variations and increased lag between temperature minimum and maximum values in the surface water and in the subsurface. Simulation of subsurface temperature and comparison with measured values hence allows D_e to be estimated.

Enhanced dispersion coefficient (D_e) estimated following this approach include both thermal conductivity ($D_{e(cond)}$) and dispersion due to advective porewater exchange ($D_{e(adv)}$). $D_{e(cond)}$ at each station can be derived from the following equation (Irvine et al., 2015; Wilson et al., 2016):

$$D_{e(cond)} = \frac{K_b}{(1-\theta)\rho_s c_s + \theta\rho_w c_w} = \frac{{K_s}^{(1-\theta)}.{K_w}^{\theta}}{(1-\theta)\rho_s c_s + \theta\rho_w c_w} \qquad (6)$$

where K_b is the bulk thermal conductivity of sediments, K_s, c_s and ρ_s are the thermal conductivity, specific heat capacity and density of the solid phase, respectively, K_w, c_w and ρ_w are the corresponding terms for the water phase and θ is the sediment porosity.

3. RESULTS

3.1. Sediment analysis

The grain size distributions of the 4 sediment cores collected in La Palme lagoon are shown in Supplementary Information (Table S1). The contents of silt and clay in sediments from Pz1, Pz2 and Pz3 were low, generally below 10-15 %. Sediments from these three sites were mainly composed of fine and medium-size sands. In contrast, sediments from Pz4 mainly comprised silt (>40 %) and had a significant clay content (> 15 %). The grain size was relatively constant with depth, with the only exception being Pz3, which included a layer (from ~30 to ~40 cm) with a higher content of silts and clays (> 20 %). Estimated sediment permeabilities from the grain size distribution and sorting following (Berg, 1970) were on the order of 10^{-10} - 10^{-11} m^2 for Pz1, Pz2 and Pz3 and 10^{-15} m^2 for Pz4. Sediments from Pz1, Pz2 and Pz3 are thus characterized by a relatively high permeability (Huettel et al., 2014), whereas Pz4 were lower permeability sediments. Average porosities (θ) were 0.47, 0.43, 0.39 and 0.70 for Pz1, Pz2, Pz3 and Pz4, respectively (Tamborski et al., 2018).

3.2. Wind, wave and lagoon water depth dynamics

The region is characterized by frequent strong winds (>10 m s^{-1}) generally blowing from the N-W (locally called “Tramontane”) and sporadic winds from the sea (S-E) that can also reach high speeds and that are usually linked to storms. Indeed, in 2017, most events where wind speed exceeded 10 m s^{-1} were blowing either from the NW (59%) or the SE (37%). The time series of wind speeds during the main period of samplings (April 2017 – December 2017) is shown in Fig 3.a.

Water depths in the lagoon decreased progressively from April to September 2017 (from ~0.9 to ~0.4 m in Pz1; Fig 3.b.), mainly as a consequence of an increase in temperatures and a reduction of precipitation and groundwater inputs that resulted in evaporative losses exceeding water inputs (Rodellas et al., 2018). During this period, wind dynamics exerted a minor control on the water depths of the lagoon and were only responsible for water depth oscillations (< 0.5 m) that lasted for less than 24 hours. Significant changes in lagoon water depths were measured between 15th-20th October (predominantly SE winds) and 6th-15th November (NW winds), as a consequence of strong wind events that opened the sandy barrier that separates the lagoon from the sea (which remained open for a few days after the wind event): lagoon water in the northern basin increased by ~0.2 m in October as a consequence of the SE wind event, which brought water from the central and southern basins (and the Mediterranean Sea), and it decreased by ~0.15 m in November due to NW winds. After these events the sandy barrier became less consolidated and thus more permeable to water exchange and most of the subsequent wind events produced significant changes in lagoon water depths.

The generation of waves in the lagoon is highly controlled by the wind regime (direction, speed and duration), as evidenced by the similar wind and wave patterns (Fig. 4). During calm periods, wave height remained below 0.02 m. Strong wind events produced rapid increases of wave heights (wave height up to 0.10 m; wave period of 1-2 s), which remained elevated for the duration of the event. No major differences in wave height and period were observed between the different sampling stations (Pz1, Pz2 and Pz3), which were located in different areas of the lagoon. The spectral analysis of lagoon water depths revealed that the influence of seiches and tides was negligible at La Palme lagoon for the

studied periods. We thus exclude them as drivers of porewater fluxes for La Palme lagoon.

3.3. Porewater salinities

Porewater could be easily sampled with a push-point piezometer from most of the depths at the locations Pz1, Pz2 and Pz3, indicating a relatively high hydraulic permeability for the sandy sediments at these locations. The only exception was a low permeability layer found at Pz3, extending from ~30 to ~40 cm below the sediment-water interface (see section 3.1.). Porewater samples could not be collected at Pz4 due to the low hydraulic conductivities, which is consistent with the low permeabilities derived from sediment core particle size analysis (see section 3.1.). Salinities in porewater mainly reflect a mixing between two endmembers (Fig. 5): i) lagoon waters with varying salinities depending on the season and the location (salinities usually between 20 and 40) and ii) deep hypersaline porewaters, with salinities above 80, most likely from an evaporative origin (Fig. 5). As a consequence, porewater salinities generally increased downwards, although these trends depend on the dynamics of this 2-endmember mixing, which varies significantly depending on the sampling time and location.

3.3.1. Estimation of advective vertical velocities from subsurface salinities

The significantly greater salinities measured in deep porewater than in shallow porewaters produce deep porewaters being significantly denser than overlying fluids (notice that temperature differences between surface and deep waters (differences < 10 ºC) have a minor influence on fluid density differences in comparison to the controls played by salinity differences). These conditions produce stable density profiles that prevent gravitational convection or salt fingering (Bokuniewicz et al., 2004; Simmons et

al., 2001). However, the variability of salinity in porewaters observed at each site during the different sampling periods (Fig. 5) suggests that porewater advection (driven by hydraulic head gradients) exerts a major control on the vertical profiles. Subsurface salinity variations can be used to assess the magnitude of porewater advection (i.e. deep porewater fluxes) and their temporal variability by applying the fluid and salt transport one-dimensional model described in section 3.2.1, which accounts for both density and hydraulic gradient differences.

The results of the observed and modeled subsurface salinities for station Pz1 are shown in Figures 6 and 7, and include both the porewater profiles collected at different periods (Fig. 6) and the continuous measurements at 30 cm below the sediment-water interface (Fig. 7). The model reproduces the observed subsurface salinities remarkably well, particularly for the observations at 30 cm below the sediment-water interface. Some differences between observed and model salinities at the shallow area of the porewater profiles might be related to mechanisms driving shallow and rapid lagoon water-porewater exchange (e.g. increase porewater fluxes driven by wave pumping or bioirrigation) that are not accounted for in the advection-dispersion model. It should also be noted that these results are also limited by the boundary conditions, which were assumed i) to vary linearly between monthly measurements at the top (continuously measured for the last ~6 months), and ii) to be constant for salinity and vary linearly over 6-months periods for pressure at the lower boundary.

The modeled vertical porewater fluxes needed to reproduce the observed subsurface salinities using the lagoon water depths and salinities measured in surface water are shown in Figure 8. Estimated porewater advection (darcy) fluxes range from -11 to 25 cm

d^{-1}, with positive fluxes representing porewater fluxes to the lagoon and negatives values the infiltration of lagoon water to the sediments. These modeled porewater advection rates for station Pz1 show a correspondence with lagoon water depths (Fig. 8): negligible or negative porewater fluxes to the lagoon occurring during periods of relatively constant and high water depths (e.g. from April to October 2017) and high upward advection rates occurring as a consequence of decreases of lagoon water depths (e.g. from July to October 2016). This pattern is consistent with the advection of deep hypersaline porewaters driven by the hydraulic gradient, largely controlled by changes on lagoon water depths: steep hydraulic gradients occur in periods of shallow lagoon water depths or after the rapid drop of lagoon water levels, leading to increased upward advection of porewaters. It should be noted that not only the absolute lagoon water depth but also the rate of change of lagoon water depths are determining the magnitude of porewater fluxes.

3.4. Subsurface temperatures and derived enhanced dispersion coefficients

For all locations (Pz1, Pz2, Pz3 and Pz4) and deployment periods (May, June and November), temperature records clearly show large amplitude daily fluctuations in surface waters (typically 3-5 ºC) (example in Fig. 9). A damping in the amplitude of diurnal temperature cycles at increasing depths is immediately apparent, as it is the phase shifting with increasing depth of measurement. Separate calibration of the numerical model within the discrete low and high wind (and wave) 48-hour periods was therefore performed to determine whether changes in wave regime induced changes in porewater exchange rate, as reflected by values of the enhanced dispersion coefficient.

3.4.1. Estimation of enhanced dispersion coefficients

The enhanced dispersion coefficient (D_e) for each of the selected 48-hour periods is determined by selecting the D_e that best fits (the lowest RMSE) the subsurface temperature records at a given depth. As an example, Fig. 10 shows the variation in RMSE vs D_e for the different 48-hour periods selected in June 2017 (temperatures at 15 cm depth at Pz1). For the two periods of low winds, best-fit values of D_e are $2.6 \cdot 10^{-2}$ m^2 d^{-1} (RMSE values of 0.15 and 0.12 ºC, respectively). For the three periods of high wind, best-fit values of D_e are $4.4 \cdot 10^{-2}$, $3.9 \cdot 10^{-2}$ and $3.2 \cdot 10^{-2}$ m^2 d^{-1} (RMSE values of 0.22, 0.19 and 0.02 ºC, respectively). Variations in the best-fit RMSE value are probably related partly to the uniformity of the wave conditions (and thus porewater exchanges and D_e) within the chosen 48-hour periods. In many cases, minimum RMSE values are close or lower than the accuracy of the sensors (0.2 ºC).

The best-fit values of D_e for each profile and each of the discrete periods (calm and windy periods) for May and June 2017 deployments, together with their uncertainties, are shown in Table 2. In some cases, modeled temperature could not fit properly the observed temperature (lowest RMSE higher than temperature sensor accuracy) and the D_e values derived from these cases are not reported.

The approach followed here to estimate dispersion coefficients from temperature time series is based on the assumption that there is no net porewater advection (no advection term in Eq. 4). The relative importance of heat transport by advective to conductive heat flux can be assessed using the dimensionless thermal Peclet Number (P_e) (Anderson, 2005; Bhaskar et al., 2012):

$$P_e = \frac{vL}{D} \qquad (7)$$

where v is porewater velocity (m d^{-1}), L is the scale length (m) and D is the dispersion coefficient (m^2 d^{-1}). Using the maximum vertical porewater fluxes derived from the fluid-salt transport model for the periods of temperature subsurface measurements (v of ~5 cm d^{-1}), an average value of the estimated enhanced dispersion coefficient under calm conditions (~0.03 m^2 d^{-1}) and using the mean grain diameter as the representative length (L = $2 \cdot 10^{-4}$ m) as suggested by Bhaskar et al. (2012), gives a thermal Peclet number of $<10^{-3}$. This value suggests a clear dominance of conductive heat transport over advective transport (Anderson, 2005). A qualitative comparison can also be performed considering the time for surface water temperature changes to propagate to the subsurface. Few hours would be required to propagate the surface temperature signal to the depths at which sensors were installed if heat transport was dominated by dispersion (e.g. ~3 hours to 15 cm below the sediment-water interface; see Eq. 5), whereas few days would be required if advection was the dominant transport mechanism (~3 days). We thus assume that the advective heat transfer will not significantly affect the interpretation of subsurface temperature data.

It should be noted that both thermal conductivity ($D_{e(cond)}$) and dispersion due to advective porewater exchange ($D_{e(adv)}$) are included within the calculated values of enhanced dispersion coefficient (D_e). The parameters used to estimate $D_{e(cond)}$ following Eq. 6 are summarized in Table 3. Note that none of these parameters are constant, since all of them depend on sediment or water specific properties (e.g. water salinity and temperature, sediment composition, grain size) and they might be highly variable (Duque et al., 2016). Thus, calculated $D_{e(cond)}$ should only be used as an approximation. Estimated $D_{e(cond)}$ range from $1.8 \cdot 10^{-2}$ m^2 d^{-1} at Pz4 (θ = 0.70) to $3.0 \cdot 10^{-2}$ m^2 d^{-1} at Pz3 (θ = 0.70). The enhanced dispersion coefficients (D_e) derived from temperature profiles for the calm

periods in May and June 2017 are in general good agreement with the theoretically calculated thermal conductivities ($D_{e(cond)}$ in Eq. 6), particularly for the stations Pz1, Pz2 and Pz3 (Fig. 11). This suggests that the porewater temperature records for calm periods are mainly governed by thermal conductivity. Notice that there is a significant disagreement between the calculated thermal conductivity and the estimated D_e for calm periods for Pz4, but these differences could be related to the used of literature-based thermal parameters instead of specific measurements for the clayey sediments of Pz4.

3.4.2. Comparison of dispersion coefficients for calm and windy conditions

As shown in Table 2 and Fig. 11, enhanced dispersion coefficients (D_e) obtained for windy 48-hour periods for a given location are generally higher than those obtained for calm periods. A Kruskal-Wallis test was applied to compare modeled enhanced dispersion coefficients for windy and calm periods (evaluating together the results from the 10 cm and 15 cm sensors for the different deployments), confirming that modeled D_e for windy periods are significantly higher than those modeled for calm periods for the deployments of May and June 2017 (Kruskal-Wallis, $p<0.01$).

When the results are clustered by locations, D_e for windy periods are consistently higher than those modeled for calm periods in all the stations (Fig. 11). The difference in D_e at each site between calm and windy periods reveals an increase of the rate of heat transport in windy periods, likely driven by enhanced porewater exchange fluxes. Assuming that the modeled D_e for the calm periods represents mainly heat transport due to thermal conductivity, the effective dispersion driven by porewater exchange ($D_{e(adv)}$) can be estimated as the difference between D_e in calm and windy periods. Estimated $D_{e(adv)}$ during the wind periods for 15 cm temperature sensors are $(1.7 \pm 0.6)\cdot10^{-2}$, (2.5 ±

0.8)·10^{-2}, (1.4 ± 0.7)·10^{-2} and (0.6 ± 0.6)·10^{-2} m^2 d^{-1} for stations Pz1, Pz2, Pz3 and Pz4 in May 2017, respectively, and (1.2 ± 0.6)·10^{-2}, (1.0 ± 1.1)·10^{-2}, (1.5 ± 1.2)·10^{-2} and (0.4 ± 0.4)·10^{-2} m^2 d^{-1} for stations Pz1, Pz2, Pz3 and Pz4 in June 2017. Slightly lower but comparable coefficients are estimated when using the temperature sensors installed at 10 cm below the sediment-water interface. The only station where dispersion driven by porewater fluxes (i.e. differences in D_e modeled for calm and windy periods) is not statistically significant is Pz4, where the presence of low-permeability sediments (permeabilities < 10^{-12} m^2) likely results in a significant reduction of porewater fluxes (Huettel et al., 2014).

4. DISCUSSION

4.1. Deep porewater fluxes to La Palme lagoon driven by oscillations of lagoon water depths: insights from porewater salinities

The hydraulic gradient between the aquifer and coastal water bodies (and its seasonal variations) is commonly a major force driving groundwater or porewater fluxes (Santos et al., 2012). Many studies have focused on the influence and variability of inland groundwater head, which is driven by the aquifer recharge (Anderson and Emanuel, 2010; Michael et al., 2005; Sugimoto et al., 2015; Yu et al., 2017), and only a limited number of studies have evaluated how changes on surface water levels in receiving water bodies alter the hydraulic gradient and, consequently, the water and solute fluxes across the land-ocean interface (Gonneea et al., 2013; Lee et al., 2013; Michael et al., 2013).

In the case of La Palme Lagoon, water depths in the lagoon are controlled by both i) seasonal changes on the balance between water inputs and evaporative losses (e.g. higher evaporation and lower water inputs in dry summer months, resulting in lower water levels in summer), and ii) wind events that control the opening of the sandy barrier and the exchange of water between the lagoon and the open sea. Changes on lagoon water depths are thus occurring over relatively short time-scales (few days-weeks), when the inland hydraulic head can be assumed to be constant. Maximum variations in coastal piezometric levels from the alluvial aquifer are indeed on the order of 30-40 cm (piezometer code BSS002LRH; ades.eaufrance.fr), occurring over annual cycles. In addition, the relatively large size of the lagoon limits the effect of variations in inland groundwater head on porewater fluxes. Lagoon water depth is thus expected to contribute more to the variability in the hydraulic gradient than variation in groundwater head does. As a consequence, in periods of decreases of lagoon water depths, the

increased hydraulic gradient favors the upward advection of deep hypersaline porewaters (porewater fluxes up to 25 cm d^{-1}), as derived from the results of the fluid-salt transport model and the measured subsurface salinities (Fig. 8). Similarly, increases of lagoon water depths may force the infiltration of lagoon waters into the sediments driven by the reduced hydraulic gradient and density convection.

4.2. Shallow porewater fluxes to La Palme lagoon driven by wind waves: insights from temperature time series

4.2.1. Drivers of increased heat transport during windy periods

A number of driving forces have been identified to produce transient porewater fluxes across the sediment-water interface, including hydraulic gradients, wave and tidal pumping, interaction of bottom currents and seafloor topography, density instabilities and pumping activities of benthic fauna (Huettel et al., 2014; Santos et al., 2012). Among all the potential drivers, short-term wind-driven wave forcing is the only mechanism that can explain the highly dynamic nature of the observed porewater fluxes with systematically higher fluxes during windy periods. As detailed in section 3.2, the strong SE and, mainly, NW winds in the area produce locally-generated wind waves that can reach significant wave heights of 5-10 cm lasting for some hours to few days.

Wave action can drive large volume of water to circulate under the swash zone, but this mechanism is only acting in the shoreline (Li and Barry, 2000; Robinson et al., 2014; Sous et al., 2016). In submerged areas, waves can also induce advective shallow porewater exchange fluxes either through pressure gradients generated by the different hydrostatic pressures between wave crests and troughs or through wave-induced oscillatory currents that interact with sediment topography (Cardenas and Jiang, 2011; Li et al.,

2017; Precht and Huettel, 2003). Wind-driven waves and currents in shallow areas can also produce shear stress inducing resuspension of sediments and increasing the magnitude of porewater exchange fluxes (Almroth-Rosell et al., 2012; Whipple et al., 2018). The magnitude of wind- (wave-) driven porewater fluxes will depend on both the physical characteristics of the water body (e.g. hydraulic conductivities of the sediments, water depths) and the magnitude of the forcing itself (i.e. wave frequency, wave amplitude, duration of the events) (Robinson et al., 2017).

Qian et al (Qian et al., 2009) developed a model to examine the effect of wave action on porewater solute profiles, which related the enhanced dispersion coefficient at the sediment surface with wave and sediment parameters:

$$D_e = \frac{5\alpha K a}{L\theta} \qquad (8)$$

where α is the hydrodynamic dispersivity (m), K is the sediment hydraulic conductivity (m d^{-1}), a is the half-wave amplitude and L is the wavelength (m). Using previously derived parameters for La Palme lagoon (α = 0.005 m; L = 1 m; K = 2-4 m d^{-1}; (Cook et al., 2018a)) and a = 0.03-0.05 m derived from wave measurements, a D_e at the sediment-water interface of $(0.4 - 1.3)\cdot10^{-2}$ m^2 d^{-1} is calculated. This range is comparable with the modeled thermal dispersion driven by porewater fluxes ($D_{e(adv)}$), suggesting that the increase in porewater flux in windy (wave) periods is consistent with wave pumping being the principal driver of porewater fluxes in La Palme lagoon.

4.2.2. Magnitude of wave-driven shallow porewater fluxes

Estimating the porewater flux required to create these modeled $D_{e(adv)}$ is not a straightforward step (Rau et al., 2014). For solute transport (as opposed to heat

transport), the dispersion coefficient (D_e) can be related to porewater flux through the hydrodynamic dispersivity (α)

$$D_e = \frac{2\overline{q_v}\alpha}{\theta} \qquad (9)$$

where $\overline{q_v}$ is the mean upward or downward flux averaged across the upwelling and downwelling phases (Anderson, 2005; Cook et al., 2018a). The calculated $\overline{q_v}$ is thus a function of the selected hydrodynamic dispersivity (α), which is a scale-dependent parameter difficult to constrain for short-scale porewater fluxes (Cook et al., 2018a). Whereas solute dispersion depends linearly on fluid velocity, the linear dependence of thermal dispersion and fluid velocity is under debate (Bhaskar et al., 2012; Molina-Giraldo et al., 2011; Rau et al., 2012). Assuming that the dispersion of heat is analogous to dispersion of a conservatively transported solute tracer in water, calculated median porewater exchange rates during windy periods would be on the order of 50 cm d^{-1} (derived from Eq. 9, using a hydrodynamic dispersivity of 0.005 m (Cook et al., 2018a; Gelhar et al., 1992)). Considering that the average water depths of La Palme lagoon usually ranges from 0.5 to 1.5 m, the porewater exchange rates estimated in this study would imply that the entire water volume of the lagoon would circulate through its sediments every 1 - 3 days, i.e. during a multi-day wind event.

King et al. (King et al., 2009) used a generalized analytical model to estimate wave-driven porewater rates on the order of 10 cm d^{-1} for a setting with characteristics similar to those from La Palme lagoon (wave amplitude of 5 cm; wave period of 1 s; water depth of 0.5 m; permeability of 10^{11} m^2). Even though these estimates from King et al. (2009) do not consider the porewater fluxes caused by the interaction of oscillatory flows and bottom topography, which may exceed those fluxes from wave pumping alone (Precht and Huettel, 2003), these rates are comparable with the advection rates roughly

estimated for wind periods in La Palme lagoon. Thus, temperature-derived porewater fluxes estimated for strong wind events in La Palme lagoon are likely a good order-of-magnitude approximation of wave-driven porewater fluxes for the studied site.

4.3. Magnitudes and temporal scales of driving forces and porewater fluxes

Recent studies conducted in La Palme lagoon have estimated average porewater fluxes to the entire lagoon to be on the order of 0.8 – 4.1 cm d^{-1} (Bejannin et al., 2017; Rodellas et al., 2018; Stieglitz et al., 2013; Tamborski et al., 2018). These fluxes, which were estimated from whole-of-lagoon radionuclide mass balances, are in good agreement with the porewater fluxes driven by oscillations of lagoon water depths estimated in this study from the fluid-salt transport model (yearly averaged porewater fluxes of 1.2 cm d^{-1}; interquartile range (q1 – q3) of -3.0 – 3.2 cm d^{-1}). Some of the whole-of-lagoon studies were conducted in calm periods with relatively high and constant lagoon waters depths (e.g. April and June 2017; (Rodellas et al., 2018)), when porewater fluxes driven by oscillations of lagoon water depths and wind-driven waves are expected to be low as inferred from subsurface salinities and temperatures. We thus cannot exclude the existence of a porewater base flux to La Palme lagoon driven by other mechanisms (e.g. bioirrigation, current-topography interactions, etc.). However, results of this study provide evidence that porewater fluxes increase significantly during periods of decreases of lagoon water depths or during strong wind events, as a consequence of increased hydraulic gradients and increased wave pumping, respectively (Fig. 12).

Importantly, the two mechanisms evaluated in this study occur over different spatial and temporal scales. At the larger scale, variations of the lagoon water depth drive deep porewater fluxes at the scale of meters. At the smaller scale, wind-driven waves force

surface water to move in and out of the shallow sediments (i.e. shallow porewater fluxes). The length of the porewater flowpath have a large influence on the biogeochemical processes occurring within sediments and on the chemical composition of porewaters discharging across the sediment-water interface (Heiss et al., 2017; Lamontagne et al., 2018; Weinstein et al., 2011). Consequently, the spatial scale of porewater fluxes needs to be considered to evaluate the overall magnitude of solute inputs driven by porewater fluxes. From a temporal perspective, porewater fluxes driven by wave pumping will only occur during important wind events, typically over periods of 1-3 days (Fig. 4). Contrarily, reduced lagoon water depths occur mainly as a consequence of the high evaporative loss in summer and/or strong wind events that control the opening of the sandy barrier and force the export of water towards the Mediterranean Sea. Periods of shallow water depths are typically extending from several days to few months (Fig. 3.b) and thus the duration of porewater fluxes forced by reduced lagoon water depths can be far larger than that of wave-induced fluxes.

A proper evaluation of the magnitude of porewater fluxes and their relevance for water systems thus requires understanding their temporal and spatial scales. As detailed in Wilson et al. (2015), most of the studies conducted elsewhere evaluating porewater fluxes are focused on specific short-term (1-5 days) samplings that only provide "snap-shot" observations and that are generally biased towards the summer field season and periods with calm conditions, when some of the driving forces (e.g. wind-waves) might not operate. Long-term observations are thus required to capture all the potential mechanisms driving porewater fluxes, including those forcings operating in sporadic intense events (e.g. storms, heavy rainfalls) (Sawyer et al., 2013; Smith et al., 2008). In addition, the driving force that is captured will also depend on the tracer technique or

approach used to estimate porewater fluxes (Cook et al., 2018b; King, 2012; Rodellas et al., 2017). Future studies in lagoons and coastal environments should focus on long-term observations and combine different tracers to capture and differentiate the fluxes produced by the diverse driving mechanisms. Long-term studies also allow isolating the driving mechanism based on temporal variations of porewater fluxes, considering periods when one forcing dominates over the other (Cook et al., 2018b), as done in this study. It should additionally be noted that the interaction between different forcings is generally nonlinear and porewater fluxes cannot be estimated simply as a sum of independent drivers (King, 2012; Yu et al., 2017). Rather, a thorough understanding of the different drivers and their interactions is required.

CONCLUSIONS

This study documents the role of lagoon water depth variations and wind-driven waves as drivers of porewater fluxes in a coastal lagoon. The dynamics of these physical driving forces are evaluated in isolation, through measurements of variations of salinity and temperature in the subsurface:

- The temporal and vertical variability of porewater salinity profiles (coupled with a fluid and salt transport model) suggests that oscillations of lagoon water depth act as a major control on the fluxes of deep (>1 m) porewaters. In periods of shallow lagoon water depths or when sudden decreases of lagoon water depths occur, the increased hydraulic gradient favors the upward advection of deep hypersaline porewaters, whereas porewater inputs are restricted (or reversed) in periods of constant and high lagoon water depths.
- The temperature records in the lagoon subsurface (coupled with a heat transport model) reveal that porewater fluxes are significantly higher in windy periods as a

consequence of locally-generated wind waves that force the circulation of lagoon waters through sediments.

Wave pumping and the hydraulic gradient contribute to significantly increase porewater fluxes to the lagoon during wind events and in periods with shallow lagoon water depths, respectively. Whereas the large fluxes driven by wave pumping only flush relatively shallow sediments and are restricted to the duration of strong wind events, porewater fluxes driven by the hydraulic gradient involve deeper sediments (> 1 m) and their relevance may extend for longer periods (up to few months). The temporal and spatial scale of porewater fluxes will largely determine the overall magnitude of solute inputs driven by porewater fluxes. An appropriate evaluation of not only the magnitude of porewater fluxes but also their underlying physical forces is thus required to fully understand the significance of these fluxes and their implications for coastal water bodies.

Acknowledgements

This research is a contribution to the ANR @RAction chair (ANR-14-ACHN-0007-01 – T Stieglitz) and Labex OT-Med (ANR-11-LABEX-0061, part of the "Investissements d'Avenir" program through the A*MIDEX project ANR-11-IDEX-0001-02) funded by the French National Research Agency (ANR). This project has received funding from the European Union's Horizon 2020 research and innovation programme under the Marie Skłodowska-Curie grant agreement No 748896. V. Rodellas acknowledges financial support from the Beatriu de Pinós postdoctoral programme of the Catalan Government (2017-BP-00334) P.G. Cook acknowledges support from IméRA (Institute of Advanced Studies), Aix-Marseille Université (Labex RFIEA and ANR ''Investissements d'avenir"). We

thank C Fleger and K Fortune from the “Parc Naturel Régional de la Narbonnaise en Méditerranée” (PNRNM; France), M David (IFREMER, BRGM, CEREGE; France), V Bailly-Comte (BRGM), P Dussouillez and J Fleury (CEREGE) for their help in sampling field trips and experimentation, as well as Wilson and C George (University of South Carolina; USA) for their recommendations on heat transport modeling. We thank A. Calafat and M. Guart (Universitat de Barcelona) for the analysis of sediment grain size distribution. We are also grateful to *GLADYS* research group (*www.gladys-littoral.org*) who supported the experimentation.

FIGURES

Figure 1. Study site (La Palme lagoon) location on the French Mediterranean coastline. The location of sampling stations (Pz1, Pz2, Pz3 and Pz4) for sediment core collection, temperature and CTD logger installation and porewater collection are shown. The position of monitoring stations (PN1, PN2 and PN3) from the "Parc Naturel Régional de la Narbonnaise en Méditerranée" (PNRNM) is also indicated.

Figure 2. Measured surface water temperatures at Pz1 between 22-26 June 2017, and modeled subsurface temperatures at 15 cm depth based on enhanced dispersion coefficients (D_e) between $1.5 \cdot 10^{-2}$ and $6.0 \cdot 10^{-2}$ m^2 d^{-1}.

Figure 3. a) Wind speeds (averaged for 6 hours) and b) water depth variations in Pz1 during the main period of samplings (April 2017 – December 2017). For simplicity, all the winds blowing from the N (270º – 90º) are represented as positive and assumed to be NW winds, and winds blowing from the S (90º – 270º) are represented as negative and assumed to be SE winds. Green and red vertical areas highlight abrupt increase or decrease, respectively, in lagoon water depths.

Figure 4. Significant wave height H_s (m) measured at stations Pz1, Pz2 and Pz3 during the three periods of deployment of temperature sensors and high-frequency pressure sensors. Hourly-averaged wind speeds (m s^{-1}) and directions (°) are also shown. Discrete 48-hour periods selected to represent both high (red vertical areas) and low (green vertical areas) wave conditions are also shown.

Figure 5. Depth profiles (in cm below the sediment-water interface) of salinity in porewater for the three piezometers collected at each campaign. Reported values at a depth of 0 correspond to the samples collected in surface waters (~10 cm above the sediment-water interface). The grey area represents the position of the layer with low permeability found at Pz3.

Figure 6. Observed and modeled porewater salinity profiles (depth in cm below the sediment-water interface) at station Pz1 from the different sampling campaigns. The grey salinity profile shown in (a) represents the linear interpolation between the measured salinities in March 2016 and the lower boundary conditions, which is used as initial concentration profile for the model.

Figure 7. Observed and modeled salinities at 30 cm below the sediment-water interface at station Pz1 for the studied period (2016-17). Observed data include porewater samples collected with piezometers ("Observed-Pz") and directly measured with the CTD logger installed in the sediments ("Observed-CTD").

Figure 8. Modeled vertical porewater fluxes (cm d^{-1}) at station Pz1, together with variations of lagoon water depths at the same station (including monthly measurements from PNRNM and continuous measurements with the CTD logger installed at surface waters). Positive porewater fluxes represent advection from sediments to surface lagoon waters.

Figure 9. Temperature records at station Pz1 for the May 2017 deployment period, including temperatures in surface waters and at different depths below the sediment-water interface.

Figure 10. Dispersion coefficient (D_e) versus RMSE for June 2017 data for the temperature sensor at 15 cm depth at Pz1. The different D_e vs RMSE curves account for the different discrete 48-hours periods selected for June 2017 temperature data (Fig. 4): 2 calm periods (Calm-J1 and Calm-J2) and 3 windy periods (Wind-J1, Wind-J2 and Wind-J3). Minimum values of RMSE for each period indicate the best-fit value of D_e. Uncertainties are defined by RMSE values 0.1 ºC greater than the minimum RMSE in each case.

Figure 11. Best-fit values of enhanced dispersion coefficients (D_e) for 15 cm temperature sensors derived from the 48-hour periods from May and June 2017 deployments. D_e reported for June 2017 represent the average (± standard deviation) of the 2 (calm) or 3 (windy) events selected during this deployment. Horizontal black lines represent the thermal conductivity estimated from Eq. 6.

Figure 12. Conceptual model describing changes on shallow and deep porewater fluxes into a coastal lagoon depending on variations of lagoon water depths and locally-generated wind waves: a) Potential base porewater flux in periods of calm, high water conditions; b) Locally-generated wind waves produce an increase of shallow porewater fluxes; c) The reduced lagoon water depths (as a consequence of high evaporation or the wind-driven outflow of lagoon waters) produce an increase of deep porewater fluxes.

.

TABLES

Table 1. Parameter values used in the one-dimensional model of subsurface salinities. Values for *h* represent the pressure head, not the total head.

Table 2. Best-fit values of enhanced dispersion coefficients for 0.10 and 0.15 m temperature sensors for discrete 48-hour periods. Units are $\cdot 10^{-2}$ m^2 d^{-1}. No simulations were conducted for loggers at stations Pz2 and Pz4 in November 2017 because water depths were too shallow and the surface sensor was often outside the water. n.r. indicates cases when the data from the logger could not be recovered.

Table 3. Parameters used for deriving thermal conductivity (Irvine et al., 2015; Wilson et al., 2016).

REFERENCES

Almroth-Rosell, E., Tengberg, A., Andersson, S., Apler, A., Hall, P.O.J., 2012. Effects of simulated natural and massive resuspension on benthic oxygen, nutrient and dissolved inorganic carbon fluxes in Loch Creran, Scotland. J. Sea Res. 72, 38–48. https://doi.org/10.1016/J.SEARES.2012.04.012

Anderson, M.P., 2005. Heat as a Ground Water Tracer. Ground Water 43, 951–968. https://doi.org/10.1111/j.1745-6584.2005.00052.x

Anderson, W.P., Emanuel, R.E., 2010. Effect of interannual climate oscillations on rates of submarine groundwater discharge. Water Resour. Res. 46. https://doi.org/10.1029/2009WR008212

Andrisoa, A., Stieglitz, T.C., Rodellas, V., Raimbault, P., 2019. Primary production in coastal lagoons supported by groundwater discharge and porewater fluxes inferred from nitrogen and carbon isotope signatures. Mar. Chem. 210, 48–60. https://doi.org/10.1016/J.MARCHEM.2019.03.003

Anschutz, P., Smith, T., Mouret, A., Deborde, J., Bujan, S., Poirier, D., Lecroart, P., 2009. Tidal sands as biogeochemical reactors. Estuar. Coast. Shelf Sci. 84, 84–90. https://doi.org/10.1016/j.ecss.2009.06.015

Bejannin, S., van Beek, P., Stieglitz, T., Souhaut, M., Tamborski, J., 2017. Combining airborne thermal infrared images and radium isotopes to study submarine groundwater discharge along the French Mediterranean coastline. J. Hydrol. Reg. Stud. 13, 72–90. https://doi.org/10.1016/J.EJRH.2017.08.001

Berg, R.R., 1970. Method for Determining Permeability from Reservoir Rock Properties 20.

Bhaskar, A.S., Harvey, J.W., Henry, E.J., 2012. Resolving hyporheic and groundwater components of streambed water flux using heat as a tracer. Water Resour. Res. 48.

https://doi.org/10.1029/2011WR011784

Boano, F., Harvey, J.W., Marion, A., Packman, A.I., Revelli, R., Ridolfi, L., Wörman, A., 2014. Hyporheic flow and transport processes: Mechanisms, models, and biogeochemical implications. Rev. Geophys. 52, 603–679. https://doi.org/10.1002/2012RG000417

Bokuniewicz, H., Pollock, M., Blum, J., Wilson, R., 2004. Submarine Ground Water Discharge and Salt Penetration Across the Sea Floor. Ground Water 42, 983–989. https://doi.org/10.1111/j.1745-6584.2004.tb02637.x

Caldwell, D.R., 1974. Thermal conductivity of sea water. Deep Sea Res. Oceanogr. Abstr. 21, 131–137. https://doi.org/10.1016/0011-7471(74)90070-9

Cardenas, M.B., Jiang, H., 2011. Wave-driven porewater and solute circulation through rippled elastic sediment under highly transient forcing. Limnol. Oceanogr. Fluids Environ. 1, 23–37. https://doi.org/10.1215/21573698-1151658

Charette, M.A., Allen, M.C., 2006. Precision Ground Water Sampling in Coastal Aquifers Using a Direct-Push, Shielded-Screen Well-Point System. Gr. Water Monit. Remediat. 26, 87–93. https://doi.org/10.1111/j.1745-6592.2006.00076.x

Cho, H.-M., Kim, G., Kwon, E.Y., Moosdorf, N., Garcia-Orellana, J., Santos, I.R., 2018. Radium tracing nutrient inputs through submarine groundwater discharge in the global ocean. Sci. Rep. 8, 2439. https://doi.org/10.1038/s41598-018-20806-2

Cook, P.G., Rodellas, V., Andrisoa, A., Stieglitz, T.C., 2018a. Exchange across the sediment-water interface quantified from porewater radon profiles. J. Hydrol. 559, 873–883. https://doi.org/10.1016/j.jhydrol.2018.02.070

Cook, P.G., Rodellas, V., Stieglitz, T.C., 2018b. Quantifying Surface Water, Porewater and Groundwater Interactions Using Tracers: Tracer Fluxes, Water Fluxes and Endmember Concentrations. Water Resour. Res. https://doi.org/10.1002/2017WR021780

Cranswick, R.H., Cook, P.G., Lamontagne, S., 2014. Hyporheic zone exchange fluxes and residence times inferred from riverbed temperature and radon data. J. Hydrol. 519, 1870–1881. https://doi.org/10.1016/J.JHYDROL.2014.09.059

Duque, C., Müller, S., Sebok, E., Haider, K., Engesgaard, P., 2016. Estimating groundwater discharge to surface waters using heat as a tracer in low flux environments: the role of thermal conductivity. Hydrol. Process. 30, 383–395. https://doi.org/10.1002/hyp.10568

Fiandrino, A., Giraud, A., Robin, S., Pinatel, C., 2012. Validation d'une méthode d'estimation des volumes d'eau échangés entre la mer et les lagunes et définition d'indicateurs hydrodynamiques associés.

Garcés, E., Basterretxea, G., Tovar-Sánchez, A., 2011. Changes in microbial communities in response to submarine groundwater input. Mar. Ecol. Prog. Ser. 438, 47–58. https://doi.org/10.3354/meps09311

Gelhar, L.W., Welty, C., Rehfeldt, K.R., 1992. A critical review of data on field-scale dispersion in aquifers. Water Resour. Res. 28, 1955–1974. https://doi.org/10.1029/92WR00607

Gobler, C., Sañudo-Wilhelmy, S., 2001. Temporal variability of groundwater seepage and brown tide blooms in a Long Island embayment. Mar. Ecol. Prog. Ser. 217, 299–309.

Gonneea, M.E., Mulligan, A.E., Charette, M.A., 2013. Climate-driven sea level anomalies modulate coastal groundwater dynamics and discharge. Geophys. Res. Lett. 40, 2701–2706. https://doi.org/10.1002/grl.50192

Heiss, J.W., Post, V.E.A., Laattoe, T., Russoniello, C.J., Michael, H.A., 2017. Physical Controls on Biogeochemical Processes in Intertidal Zones of Beach Aquifers. Water Resour. Res. 53, 9225–9244. https://doi.org/10.1002/2017WR021110

Huettel, M., Berg, P., Kostka, J.E., 2014. Benthic exchange and biogeochemical cycling in

permeable sediments. Ann. Rev. Mar. Sci. 6, 23–51. https://doi.org/10.1146/annurev-marine-051413-012706

Hwang, D.W., Lee, Y.W., Kim, G., 2005. Large submarine groundwater discharge and benthic eutrophication in Bangdu Bay on volcanic Jeju Island, Korea. Limnol. Oceanogr. 50, 1393–1403.

Irvine, D., Simmons, C., Werner, A., Graf, T., 2015. Heat and solute tracers: how do they compare in heterogeneous aquifers? Ground Water 53, 10–20. https://doi.org/10.1111/gwat.12146

Johnson, A.N., Boer, B.R., Woessner, W.W., Stanford, J.A., Poole, G.C., Thomas, S.A., O'Daniel, S.J., 2005. Evaluation of an Inexpensive Small-Diameter Temperature Logger for Documenting Ground Water-River Interactions. Gr. Water Monit. Remediat. 25, 68–74. https://doi.org/10.1111/j.1745-6592.2005.00049.x

King, J.N., 2012. Synthesis of benthic flux components in the Patos Lagoon coastal zone, Rio Grande do Sul, Brazil. Water Resour. Res. 48. https://doi.org/10.1029/2011WR011477

King, J.N., Mehta, A.J., Dean, R.G., 2009. Generalized analytical model for benthic water flux forced by surface gravity waves. J. Geophys. Res. 114, C04004. https://doi.org/10.1029/2008JC005116

Kwon, E.Y., Kim, G., Primeau, F., Moore, W.S., Cho, H.-M., DeVries, T., Sarmiento, J.L., Charette, M.A., Cho, Y.-K., 2014. Global estimate of submarine groundwater discharge based on an observationally constrained radium isotope model. Geophys. Res. Lett. n/a-n/a. https://doi.org/10.1002/2014GL061574

Lamontagne, S., Cosme, F., Minard, A., Holloway, A., 2018. Nitrogen attenuation, dilution and recycling in the intertidal hyporheic zone of a subtropical estuary. Hydrol. Earth Syst. Sci. 22, 4083–4096. https://doi.org/10.5194/hess-22-4083-2018

Lee, E., Hyun, Y., Lee, K.-K., 2013. Sea level periodic change and its impact on submarine groundwater discharge rate in coastal aquifer. Estuar. Coast. Shelf Sci. 121–122, 51–60. https://doi.org/10.1016/j.ecss.2013.02.011

Lee, Y.W., Kim, G., Lim, W.A., Hwang, D.W., 2010. A relationship between submarine groundwater-borne nutrients traced by Ra isotopes and the intensity of dinoflagellate red-tides occurring in the southern sea of Korea. Limnol. Oceanogr. 55, 1–10.

Li, L., Barry, D.., 2000. Wave-induced beach groundwater flow. Adv. Water Resour. 23, 325–337. https://doi.org/10.1016/S0309-1708(99)00032-9

Li, Y., Šimůnek, J., Wang, S., Zhang, W., Yuan, J., 2017. Simulating the Effects of Lake Wind Waves on Water and Solute Exchange across the Lakeshore Using Hydrus-2D. Water 9, 566. https://doi.org/10.3390/w9080566

Liefer, J.D., MacIntyre, H.L., Su, N., Burnett, W.C., 2013. Seasonal Alternation Between Groundwater Discharge and Benthic Coupling as Nutrient Sources in a Shallow Coastal Lagoon. Estuaries and Coasts 37, 1–16. https://doi.org/10.1007/s12237-013-9739-4

Martin, J.B., Cable, J.E., Jaeger, J., Hartl, K., Smith, C.G., 2006. Thermal and chemical evidence for rapid water exchange across the sediment-water interface by bioirrigation in the Indian River Lagoon, Florida. Limnol. Oceanogr. 51, 1332–1341. https://doi.org/10.4319/lo.2006.51.3.1332

Martin, J.B., Cable, J.E., Smith, C., Roy, M., Cherrier, J., 2007. Magnitudes of submarine groundwater discharge from marine and terrestrial sources: Indian River Lagoon, Florida. Water Resour. Res. 43, n/a-n/a. https://doi.org/10.1029/2006WR005266

Martin, J.B., Cable, J.E., Swarzenski, P.W., Lindenberg, M.K., 2004. Enhanced Submarine Ground Water Discharge from Mixing of Pore Water and Estuarine Water. Ground

Water 42, 1000–1010. https://doi.org/10.1111/j.1745-6584.2004.tb02639.x

Michael, H.A., Mulligan, A.E., Harvey, C.F., 2005. Seasonal oscillations in water exchange between aquifers and the coastal ocean. Nature 436, 1145–8. https://doi.org/10.1038/nature03935

Michael, H.A., Russoniello, C.J., Byron, L.A., 2013. Global assessment of vulnerability to sea-level rise in topography-limited and recharge-limited coastal groundwater systems. Water Resour. Res. 49, 2228–2240. https://doi.org/10.1002/wrcr.20213

Molina-Giraldo, N., Bayer, P., Thermal, P.B.-I.J. of, 2011, undefined, 2011. Evaluating the influence of thermal dispersion on temperature plumes from geothermal systems using analytical solutions. Int. J. Therm. Sci. 50, 1223–1231. https://doi.org/doi.org/10.1016/j.ijthermalsci.2011.02.004

Moore, W.S., 2010. The Effect of Submarine Groundwater Discharge on the Ocean. Ann. Rev. Mar. Sci. 2, 59–88. https://doi.org/10.1146/annurev-marine-120308-081019

Moore, W.S., Sarmiento, J.L., Key, R.M., 2008. Submarine groundwater discharge revealed by 228Ra distribution in the upper Atlantic Ocean. Nat. Geosci. 1, 309–311. https://doi.org/10.1038/ngeo183

Morris, J.T., 1995. The Mass Balance of Salt and Water in Intertidal Sediments: Results from North Inlet, South Carolina. Estuaries 18, 556. https://doi.org/10.2307/1352376

Nash, S.G., 1984. Newton-Type Minimization via the Lanczos Method. SIAM J. Numer. Anal. 21, 770–788. https://doi.org/10.1137/0721052

Oliphant, T.E., 2007. Python for Scientific Computing. Comput. Sci. Eng. 9, 10–20. https://doi.org/10.1109/MCSE.2007.58

Paerl, H., 1997. Coastal eutrophication and harmful algal blooms: Importance of atmospheric deposition and groundwater as" new" nitrogen and other nutrient

sources. Limnol. Oceanogr. 42, 1154–65.

Precht, E., Huettel, M., 2003. Advective pore-water exchange driven by surface gravity waves and its ecological implications. Limnol. Oceanogr. 48, 1674–1684. https://doi.org/10.4319/lo.2003.48.4.1674

Qian, Q., Clark, J.J., Voller, V.R., Stefan, H.G., 2009. Depth-Dependent Dispersion Coefficient for Modeling of Vertical Solute Exchange in a Lake Bed under Surface Waves. J. Hydraul. Eng. 135, 187–197. https://doi.org/10.1061/(ASCE)0733-9429(2009)135:3(187)

Rapaglia, J.P., Bokuniewicz, H.J., 2009. The effect of groundwater advection on salinity in pore waters of permeable sediments. Limnol. Oceanogr. 54, 630–643.

Rau, G.C., Andersen, M.S., Acworth, R.I., 2012. Experimental investigation of the thermal dispersivity term and its significance in the heat transport equation for flow in sediments. Water Resour. Res. 48. https://doi.org/10.1029/2011WR011038

Rau, G.C., Andersen, M.S., McCallum, A.M., Roshan, H., Acworth, R.I., 2014. Heat as a tracer to quantify water flow in near-surface sediments. Earth-Science Rev. 129, 40–58. https://doi.org/10.1016/J.EARSCIREV.2013.10.015

Robinson, C., Xin, P., Li, L., Barry, D.A., 2014. Groundwater flow and salt transport in a subterranean estuary driven by intensified wave conditions. Water Resour. Res. 50, 165–181. https://doi.org/10.1002/2013WR013813

Robinson, C.E., Xin, P., Santos, I.R., Charette, M.A., Li, L., Barry, D.A., 2017. Groundwater dynamics in subterranean estuaries of coastal unconfined aquifers: Controls on submarine groundwater discharge and chemical inputs to the ocean. Adv. Water Resour. https://doi.org/10.1016/J.ADVWATRES.2017.10.041

Rodellas, V., Garcia-Orellana, J., Masqué, P., Feldman, M., Weinstein, Y., 2015. Submarine groundwater discharge as a major source of nutrients to the Mediterranean Sea.

Proc. Natl. Acad. Sci. U. S. A. 112, 3926–30. https://doi.org/10.1073/pnas.1419049112

Rodellas, V., Garcia-Orellana, J., Trezzi, G., Masqué, P., Stieglitz, T.C., Bokuniewicz, H., Cochran, J.K., Berdalet, E., 2017. Using the radium quartet to quantify submarine groundwater discharge and porewater exchange. Geochim. Cosmochim. Acta 196. https://doi.org/10.1016/j.gca.2016.09.016

Rodellas, V., Stieglitz, T.C., Andrisoa, A., Cook, P.G., Raimbault, P., Tamborski, J.J., van Beek, P., Radakovitch, O., 2018. Groundwater-driven nutrient inputs to coastal lagoons: The relevance of lagoon water recirculation as a conveyor of dissolved nutrients. Sci. Total Environ. 642, 764–780. https://doi.org/10.1016/j.scitotenv.2018.06.095

Santos, I.R., Burnett, W.C., Chanton, J., Dimova, N., Peterson, R.N., 2009. Land or ocean?: Assessing the driving forces of submarine groundwater discharge at a coastal site in the Gulf of Mexico. J. Geophys. Res. 114, C04012. https://doi.org/10.1029/2008JC005038

Santos, I.R., Eyre, B.D., Huettel, M., 2012. The driving forces of porewater and groundwater flow in permeable coastal sediments: A review. Estuar. Coast. Shelf Sci. 98, 1–15. https://doi.org/10.1016/j.ecss.2011.10.024

Savidge, W.B., Wilson, A., Woodward, G., 2016. Using a Thermal Proxy to Examine Sediment–Water Exchange in Mid-Continental Shelf Sandy Sediments. Aquat. Geochemistry 22, 419–441. https://doi.org/10.1007/s10498-016-9295-1

Sawyer, A.H., Shi, F., Kirby, J.T., Michael, H.A., 2013. Dynamic response of surface water-groundwater exchange to currents, tides, and waves in a shallow estuary. J. Geophys. Res. Ocean. 118, 1749–1758. https://doi.org/10.1002/jgrc.20154

Simmons, C.T., Fenstemaker, T.R., Sharp, J.M., 2001. Variable-density groundwater flow and solute transport in heterogeneous porous media: approaches, resolutions and

future challenges. J. Contam. Hydrol. 52, 245–275. https://doi.org/10.1016/S0169-7722(01)00160-7

Smith, C.G., Cable, J.E., .Martin, J.B., 2008. Episodic high intensity mixing events in a subterranean estuary: Effects of tropical cyclones. Limnol. Oceanogr. 53, 666–674. https://doi.org/10.4319/lo.2008.53.2.0666

Sous, D., Petitjean, L., Bouchette, F., Rey, V., Meulé, S., Sabatier, F., Martins, K., 2016. Field evidence of swash groundwater circulation in the microtidal rousty beach, France. Adv. Water Resour. 97, 144–155. https://doi.org/10.1016/J.ADVWATRES.2016.09.009

Stieglitz, T.C., Beek, P., Souhaut, M., Cook, P.G., 2013. Karstic groundwater discharge and seawater recirculation through sediments in shallow coastal Mediterranean lagoons, determined from water, salt and radon budgets. Mar. Chem. 156, 73–84. https://doi.org/10.1016/j.marchem.2013.05.005

Sugimoto, R., Honda, H., Kobayashi, S., Takao, Y., Tahara, D., Tominaga, O., Taniguchi, M., 2015. Seasonal Changes in Submarine Groundwater Discharge and Associated Nutrient Transport into a Tideless Semi-enclosed Embayment (Obama Bay, Japan). Estuaries and Coasts. https://doi.org/10.1007/s12237-015-9986-7

Tamborski, J., Bejannin, S., Garcia-Orellana, J., Souhaut, M., Charbonnier, C., Anschutz, P., Pujo-Pay, M., Conan, P., Crispi, O., Monnin, C., Stieglitz, T., Rodellas, V., Andrisoa, A., Claude, C., van Beek, P., 2018. A comparison between water circulation and terrestrially-driven dissolved silica fluxes to the Mediterranean Sea traced using radium isotopes. Geochim. Cosmochim. Acta 238, 496–515. https://doi.org/10.1016/J.GCA.2018.07.022

Valiela, I., Costa, J., Foreman, K., Teal, J.M., Howes, B., Aubrey, D., 1990. Transport of groundwater-borne nutrients from watersheds and their effects on coastal waters.

Biogeochemistry 10, 177–197. https://doi.org/10.1007/BF00003143

van der Walt, S.S., Colbert, S.C., Varoquaux, G.G., 2011. The NumPy Array: A Structure for Efficient Numerical Computation. Comput. Sci. Eng. 13, 22–30. https://doi.org/10.1109/MCSE.2011.37

Voss, C.I., Souza, W.R., 1987. Variable density flow and solute transport simulation of regional aquifers containing a narrow freshwater-saltwater transition zone. Water Resour. Res. 23, 1851–1866. https://doi.org/10.1029/WR023i010p01851

Weinstein, Y., Yechieli, Y., Shalem, Y., Burnett, W.C., Swarzenski, P.W., Herut, B., 2011. What is the role of fresh groundwater and recirculated seawater in conveying nutrients to the coastal ocean? Environ. Sci. Technol. 45, 5195–200. https://doi.org/10.1021/es104394r

Whipple, A.C., Luettich, R.A., Reynolds-Fleming, J. V., Neve, R.H., 2018. Spatial differences in wind-driven sediment resuspension in a shallow, coastal estuary. Estuar. Coast. Shelf Sci. 213, 49–60. https://doi.org/10.1016/J.ECSS.2018.08.005

Wilke, M., Boutière, H., 2000. Synthèse générale du fonctionnement hydrobiologique de l'étang de La Palme, CEH. Perpignan, France.

Wilson, A.M., Evans, T.B., Moore, W.S., Schutte, C.A., Joye, S.B., 2015. What time scales are important for monitoring tidally influenced submarine groundwater discharge? Insights from a salt marsh. Water Resour. Res. 51, 4198–4207. https://doi.org/10.1002/2014WR015984

Wilson, A.M., Woodward, G.L., Savidge, W.B., 2016. Using heat as a tracer to estimate the depth of rapid porewater advection below the sediment–water interface. J. Hydrol. 538, 743–753. https://doi.org/10.1016/j.jhydrol.2016.04.047

Yu, X., Xin, P., Lu, C., Robinson, C., Li, L., Barry, D.A., 2017. Effects of episodic rainfall on a subterranean estuary. Water Resour. Res. 53, 5774–5787.

https://doi.org/10.1002/2017WR020809

TABLE 1

Parameter	Units	Specified value	Allowable range	Calibrated value
h_{top}	m	0 - 0.91*	-	-
h_{bot}	m	-	3.0 - 5.0	Day 0: 4.32 Day 182: 4.24 Day 365: 4. 80 Day 547: 4.17 Day 730: 4.13
C_{top}	-	16.8 - 35.9 *	-	-
C_{bot}	-	-	90 - 130	100
k	m^2	-	10^{-13} - 10^{-12}	$1.63 \cdot 10^{-12}$**
μ	$Pa\ s$	$8.9 \cdot 10^{-4}$	-	-
$\partial\rho/\partial C$	-	0.77	-	-
θ	-	-	0.4 - 0. 5	0.40
S_{op}	Pa^{-1}	$1 \cdot 10^{-8}$	-	-
α	m	-	0.2 - 1.0	0.2
D_M	$m^2\ s^{-1}$	$1.16 \cdot 10^{-9}$	-	-

** Taken from measurements in the Lagoon (at stations Pz1 and PN1).*

*** Corresponds to a hydraulic conductivity of 1.55 m d^{-1} for non-saline water.*

TABLE 2

		Sensor at 10 cm			Sensor at 15 cm		
Event Numb	**Pz**	**Best_10cm**	**-Δ**	**+Δ**	**Best-15cm**	**-Δ**	**+Δ**
May 17							
Calm-M1	PZ1	**2.3**	0.4	0.5	**2.2**	0.4	0.4
Calm-M1	PZ2	**3.0**	0.5	0.6	**2.3**	0.3	0.4
Calm-M1	PZ3	**2.8**	0.4	0.5	**2.8**	0.4	0.4
Calm-M1	PZ4	**3.1**	0.5	0.5	**3.1**	0.4	0.4
Wind-M1	PZ1	**3.3**	0.4	0.5	**3.9**	0.5	0.5
Wind-M1	PZ2	**4.0**	0.5	0.6	**4.8**	0.6	0.8
Wind-M1	PZ3	**3.8**	0.5	0.6	**4.2**	0.5	0.6
Wind-M1	PZ4	**3.3**	0.4	0.5	**3.7**	0.4	0.5
June 17							
Calm-J1	PZ1	**n.r.**			**2.6**	0.8	1.1
Calm-J2	PZ1	**n.r.**			**2.6**	0.5	0.7
Calm-J1	PZ2	**2.7**	0.5	0.5	**3.1**	0.5	0.6
Calm-J2	PZ2	**2.5**	0.4	0.4	**2.7**	0.4	0.4
Calm-J1	PZ3	**2.5**	0.6	0.7	**3.2**	0.6	0.8
Calm-J2	PZ3	**2.4**	0.4	0.4	**2.8**	0.4	0.4
Calm-J1	PZ4	**n.r.**			**3.4**	0.5	0.6
Calm-J2	PZ4	**n.r.**			**3.0**	0.4	0.5
Wind-J1	PZ1	**n.r.**			**4.4**	0.6	0.7
Wind-J2	PZ1	**n.r.**			**3.9**	0.6	0.7
Wind-J3	PZ1	**n.r.**			**3.2**	0.6	0.7
Wind-J1	PZ2	**4.0**	0.5	0.6	**4.8**	0.6	0.8
Wind-J2	PZ2	**3.4**	0.5	0.6	**4.0**	0.6	0.8
Wind-J3	PZ2	**2.6**	0.6	0.7	**2.7**	0.6	0.8
Wind-J1	PZ3	**4.1**	0.6	0.8	**5.4**	0.9	1.1
Wind-J2	PZ3	**3.9**	0.6	0.7	**4.9**	0.8	0.9
Wind-J3	PZ3	**2.6**	0.6	0.8	**3.1**	0.7	0.9
Wind-J1	PZ4	**n.r.**			**3.8**	0.5	0.7
Wind-J2	PZ4	**n.r.**			**3.6**	0.5	0.6
Wind-J3	PZ4	**n.r.**			**3.3**	0.6	0.7

TABLE 3

Parameter	Symbol	Value	Units
Density of water	ρ_w	1025	kg m^{-3}
Density of solids	ρ_s	2650	kg m^{-3}
Specific heat capacity of water	c_w	4180	J kg^{-1} ºC^{-1}
Specific heat capacity of solids	c_s	1170	J kg^{-1} ºC^{-1}
Thermal conductivity of water	K_w	0.57	J s^{-1} m^{-1} ºC^{-1}
Thermal conductivity of solids	K_s	2.0	J s^{-1} m^{-1} ºC^{-1}

HIGHLIGHTS

- Lagoon water depth oscillations drive deep porewater fluxes
- Locally-generated wind waves drive shallow porewater fluxes
- Wind waves and lagoon water depth variations are major driving forces
- Spatial and temporal scales of drivers determine the relevance of porewater fluxes